CONTRIBUTED
P A P E R

Palomar Receive Terminal (PRT) for the Mars Laser Communication Demonstration (MLCD) Project

A laser communications link to transmit science, telemetry and test data from Mars to the Earth has been designed; the next step will be technology validation demonstrations.

By Abhijit Biswas, Bruce Moision, William T. Roberts, William H. Farr, Andrew Gray, Kevin Quirk, Jon Hamkins, Michael K. Cheng, Jonathan Gin, Michael Nakashima, Gerardo G. Ortiz, Sabino Piazzolla, Carl Christian Liebe, and David L. Losh

ABSTRACT | Significant technological advances were made toward utilizing the Hale telescope for receiving the faint laser communication signals transmitted from an optical transceiver on a spacecraft orbiting Mars. The so-called Palomar Receive Terminal design, which would have supported nominal downlink data rates of 1–30 Mbps, is described. Testing to validate technologies for near-Sun (3° from edge of solar disc) daytime operations is also discussed. Finally, a laboratory end-to-end link utilizing a 64-ary pulse-position modulated photon-counting receiver and decoder that achieved predicted near-capacity (within 1.4 dB) performance is described.

KEYWORDS | Deep space; laser communication; photon counting; pulse-position modulation

I. INTRODUCTION

The Mars Laser Communication Demonstration (MLCD) Project [1]–[4] was established with the intent of demonstrating the first ever Mars-to-Earth laser communication link. An optical flight transceiver called the Mars Laser Terminal [5], [6] (MLT) onboard the Mars Telecommunication Orbiter (MTO) [7] was to transmit science, telemetry, and test data to the MLCD Ground Network (MGN) at nominal data rates varying from 1 to 30 Mbps. The MGN consisted of the Palomar Receive Terminal (PRT) [8] and the Link Development and Evaluation System (LDES) [9], [10]. The 5.08-m-diameter Hale telescope at Palomar Observatory, Palomar Mountain, CA, retrofitted with a photon-counting receiver, would have served as the PRT. Following a successful preliminary design, the MLCD Project was discontinued due to programmatic changes within NASA that resulted in a cancellation of MTO. In this paper, we will describe the preliminary design of the PRT with an emphasis on the driving technologies that will continue to be of interest for future demonstrations of deep-space laser communication.

An overview of PRT with its relation to the link design is provided in Section II, followed by a brief description of the major assemblies in Section III. In Section IV, critical technology validation test results are presented, followed by conclusions in Section V.

II. SYSTEM BLOCK DIAGRAM

Fig. 1 shows the system block diagram for the PRT with different colored blocks representing the major assemblies. The primary purpose of the solar rejection filter

Manuscript received January 22, 2007; revised April 18, 2007. This work was supported by the National Aeronautics and Space Administration.
The authors are with the Jet Propulsion Laboratory, California Institute of Technology, Pasadena, CA 91109 USA (e-mail: Abhijit.Biswas@jpl.nasa.gov; Bruce.E.Moision@jpl.nasa.gov; William.T.Roberts@jpl.nasa.gov; William.H.Farr@jpl.nasa.gov; Andrew.A.Gray@jpl.nasa.gov; Kevin.J.Quirk@jpl.nasa.gov; Jon.Hamkins@jpl.nasa.gov; Michael.K.Cheng@jpl.nasa.gov; Jonathan.W.Gin@jpl.nasa.gov; Michael.A.Nakashima@jpl.nasa.gov; Gerardo.G.Ortiz@jpl.nasa.gov; Sabino.Piazzolla@jpl.nasa.gov; Carl.C.Liebe@jpl.nasa.gov; David.L.Losh@jpl.nasa.gov).
Digital Object Identifier: 10.1109/JPROC.2007.905054

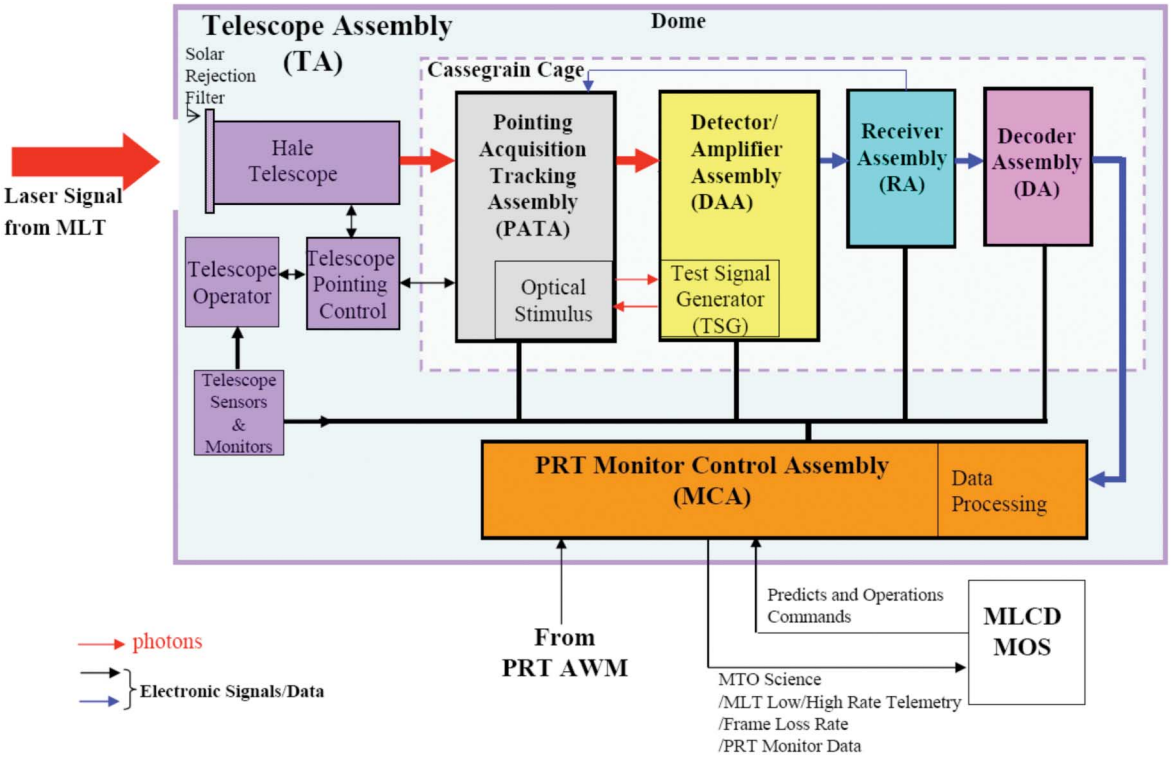

Fig. 1. ***System block diagram for PRT. The different colors are indicative of the partitioning of the PRT major assemblies.***

(SRF) was to protect the Hale telescope while receiving downlink during near Sun operations, i.e., less than 40° Sun-Earth-probe (SEP) angle. Light gathered at the Hale telescope Cassegrain focus would be coupled to the pointing acquisition and tracking assembly (PATA) where spatial and spectral acquisition is accomplished prior to the photons' being incident on the detector amplifier assembly (DAA). Photoelectric conversion at the DAA with the output signal being fed to the receiver assembly (RA) would follow. Temporal acquisition to determine slot, symbol, and frame boundaries would be performed by the RA with the temporally acquired signal being passed to the decoder. Estimates of the transmitted block of bits, or an error flag, would be produced after decoding. State control, status monitoring, data processing, archival, and coordination with the MLCD Mission Operations System (MOS) would be carried out by the monitor and control assembly (MCA). The MCA would also coordinate link activities with the local atmosphere and weather monitoring (AWM) station. The optical stimulus in the PATA and the test signal generator in the DAA were used for calibration and testing of the system in the absence of a downlink laser signal.

Derivation of the photon budget [11] and selection of modulation and coding schemes [12] for an optical downlink from Mars were described earlier. A photon flux (photons/second) composed of signal (λ_s) and background noise (λ_b) is incident at the PRT DAA. The incident $(\lambda_s + \lambda_b)$ depends upon the distance of the transmitter, the SEP angle, and prevailing atmospheric conditions, i.e., attenuation, sky radiance, and turbulence. For a given set of conditions, the operating point can be optimized by spatial filtering, i.e., varying the detector field-of-view (FOV). To clarify, when background photon flux incident on the detector is low, widening the FOV to collect close to 100% of the signal provides the best operating point. However, with the same atmospheric turbulence and high background photon flux, reducing the FOV to detect a smaller fraction of the signal may improve performance because of reduced noise penalty from "in-band" background light.

Fig. 2 illustrates a mapping of incident signal and noise pairs in decibel-photons/nanosecond to partitions (blue lines) of achievable throughputs in Mbps, optimized under the constraints that the pulse-position modulation (PPM) alphabet size is chosen from {32, 64}, and the slot-width (T_s) is a multiple of 1.6 ns (inverse of the clock rate implemented on MLT). The partitions are overlaid with a representative range of pairs for "design" conditions (red curve) on the MLCD link. To obtain the mapping, the incident signal and noise powers are first decreased by 5.23 dB to account for a photodetection efficiency of 0.3, and the signal rate is decreased by an additional 5 dB to allow for margin and implementation losses, yielding estimated photon rates at the DAA. The partitions correspond to the capacity of the channel with these signal and noise pairs. In [13], a point design representing a nominal MLCD link budget for a signal received with PRT when the MLT transmits from the

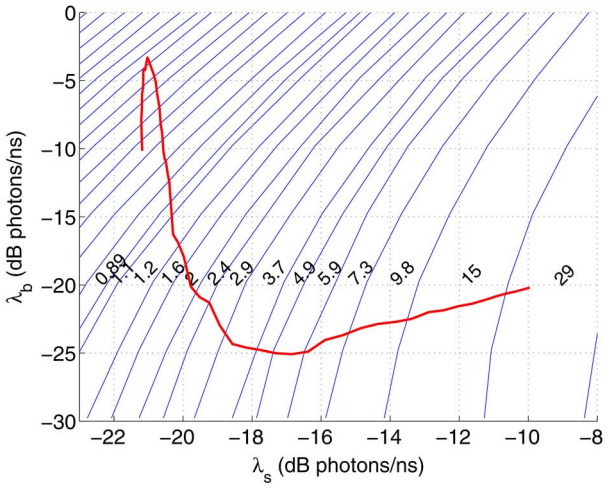

Fig. 2. *Incident signal and noise power pairs mapped to partitions (blue lines) of achievable throughputs in Mbps. Red curve overlaying the partitions represents anticipated pairs under design conditions. A data point corresponding to the budget presented in [13] is also shown with a red asterisk.*

maximum Mars distance is presented. This operating point is shown with a red asterisk in Fig. 2.

III. PRT DESCRIPTION

A brief description of the assemblies in the PRT follows.

A. Telescope Assembly

A detailed survey of existing telescopes was conducted prior to selecting the Hale telescope. Key considerations were:

1) sufficient collection aperture diameter to satisfy required data rates;
2) ability to operate during the day at low SEP angles (down to 3°);
3) favorable topography from cloud cover and atmospheric turbulence;
4) existing developed infrastructure;
5) proximity to potential uplink telescopes needed to transmit laser beacons.

Alternate contenders were the Infra-Red Telescope Facility (IRTF) and Keck telescopes at Mauna Kea. The high rental cost of Keck and expensive upgrades for using IRTF eliminated them from further consideration. Studies conducted by Caltech Optical Observatories confirmed the feasibility of using the Hale telescope with viable approaches to satisfy the 3° SEP angle requirement.

The elements of the TA were shown in purple shading in Fig. 1. The key requirements were:

i) to enable link operations at SEP angles of less than 3°;
ii) to provide a system bidirectional scatter distribution function (BSDF) of less than 0.08 sr^{-1};
iii) to transmit at least 78% of 1064 nm light;
iv) to restrict blurring by the solar rejection filter to less than 15 μrad.

The main design and development item for the TA was to provide solar protection [14], [15] since all other elements of the Hale telescope were operational.

An SRF was selected instead of baffles, primarily because at low SEP angles, the baffles had a high transmission of stray background light due to near grazing incidence. Though installation of the SRF over the dome slit would have provided isolation of the dome interior from the ambient atmosphere, as a cost saving measure, installation of the SRF at the entrance aperture was selected. Fig. 3(a) shows a solid-model rendering of the Hale telescope with the filter placement design in Fig. 3(b). A shroud [Fig. 3(c)] was designed to protect the primary mirror from incident off-axis sunlight through the sides of the open structure.

The final design selected for the SRF was a clear polyimide 1 (CP1) substrate developed at Langley Research Center [16] over the alternative, more expensive glass-panel mosaic approach. With good optical and mechanical characteristics, CP1 could be cast in 1.5-m pieces. This substrate offered good scattering characteristics, was amenable to cleaning for maintaining BSDF against dust buildup, and displayed no observable birefringence. Furthermore, ready availability coupled with an order of magnitude lower cost favored the membrane filter. Its light weight also offered ease of deployment and removal. Safety concerns from possible breakage of glass panels while the filter was deployed were also overcome with the membrane SRF.

The front of the filter, shown in Fig. 4, was an all-dielectric stack of alternating layers of high- and low-index films, designed to efficiently reflect visible light from 350 to 1000 nm. This is necessary on the front side to prevent the absorption of a significant amount of sunlight by the filter. On the back side of the substrate film, an "induced transmission" filter was applied. This filter makes use of a very thin layer of metal as the primary rejection agent. By placing a dielectric stack on each side of the metal layer, light at one narrow wavelength band can efficiently be coupled into and out of the metal. By keeping the metal layer thin, the loss from intrinsic absorption by the metal layer could be restricted to less than 1 dB while achieving an average of 10–15 dB attenuation at other wavelengths.

B. Pointing Acquisition Tracking Assembly (PATA)

The key functional requirements for PATA were:

i) to optically reimage light from the Cassegrain focus of the Hale telescope on to the DAA with an overall transmission loss of less than 3 dB;
ii) to implement a line-of-sight stabilization loop that would maintain the focal spot on the detector against atmospheric perturbations and telescope jitter;

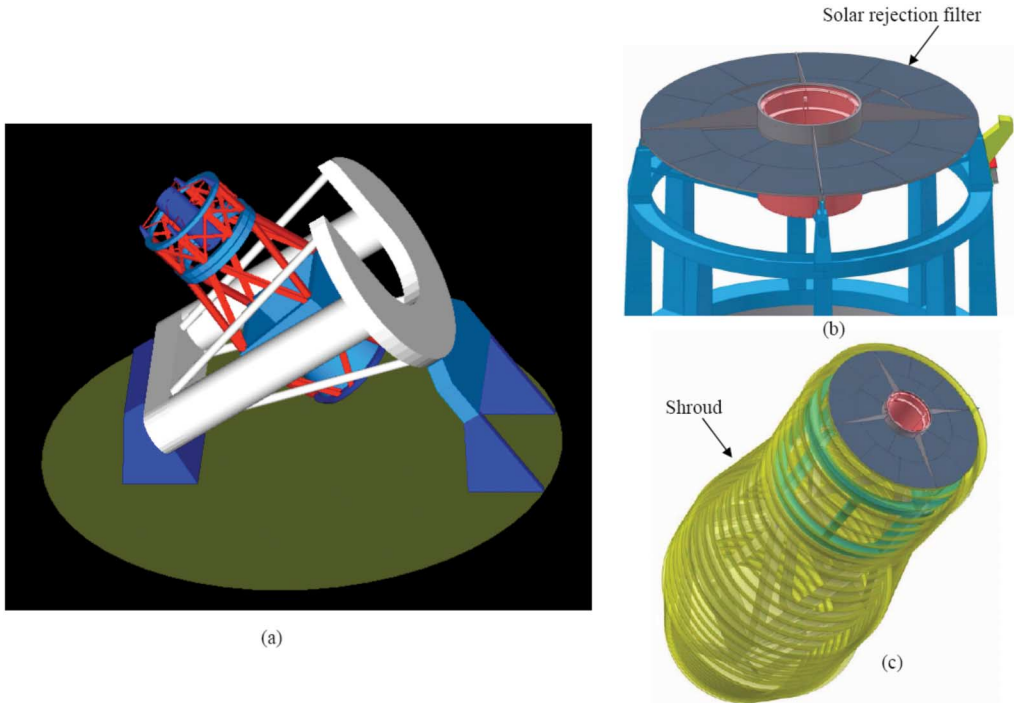

Fig. 3. *(a) Solid model rendering of the Hale telescope showing the horseshoe shaped right-ascension wheel and the open frame structure of the telescope. (b) Filter placement design near the head ring assembly of the telescope. (c) Shroud design to prevent side solar illumination of the primary mirror.*

iii) to provide 0.1 nm noise equivalent bandwidth (NEB) filtering of signal prior to incidence on the detector;
iv) to provide state control and relay component status to the MCA;
v) to support validation of all PATA functions in the absence of a downlink laser signal, i.e., to provide a built-in self-test capability for alignment and calibration of PRT.

The block diagram in Fig. 5 shows the essentials of the PATA design [17]. The primary receive light path is shown by a solid green line. Alternative light paths used to assist acquisition, or for calibration and testing, are shown by a dashed green line. The red dashed line shows the optical path used for alignment. Dashed black lines show all the control signals for various actuators and test equipment. Blue-filled boxes are optics and controllers, purple-filled boxes indicate the optical stimulus, and yellow-filled boxes indicate interfacing neighbors. The signal and background from the Hale telescope Cassegrain focus would be recollimated and folded onto an optical breadboard or custom interface plate. The circularly polarized downlink laser would be linearized and incident on a steering mirror located at a conjugate pupil. During initial acquisition, the signal would be directed to a coarse field-of-view acquisition sensor shown by a dashed green path following the polarizing beam splitter. Initial acquisition would rely on blind pointing the Hale telescope using MTO spacecraft ephemeredes. The acquisition sensor FOV would cover the blind pointing uncertainty. After verifying initial coarse spatial acquisition in a 1-nm NEB filter, the downlink path would be switched toward the 0.1-nm NEB filter shown in Fig. 5. Temperature control would tune out uncertainties in received laser wavelength due to Doppler shifts and drifts in the MLT transmitter. During initial spectral acquisition, the field-stop would be wide open ($\sim 50 - \mu$rad) and photons would be incident on the photon-counting quadrant detector (see Section III-C). The outputs from the quadrant would be fed to the receiver assembly where temporal acquisition, i.e., determination of the PPM slot, symbol, and frame boundaries would

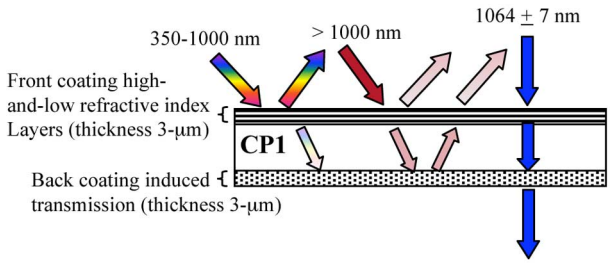

Fig. 4. *The front surface reflects visible wavelengths, whereas the back surface reflects and absorbs visible and infrared wavelengths. The filter theoretical design predicted 94% transmission at 1064 nm.*

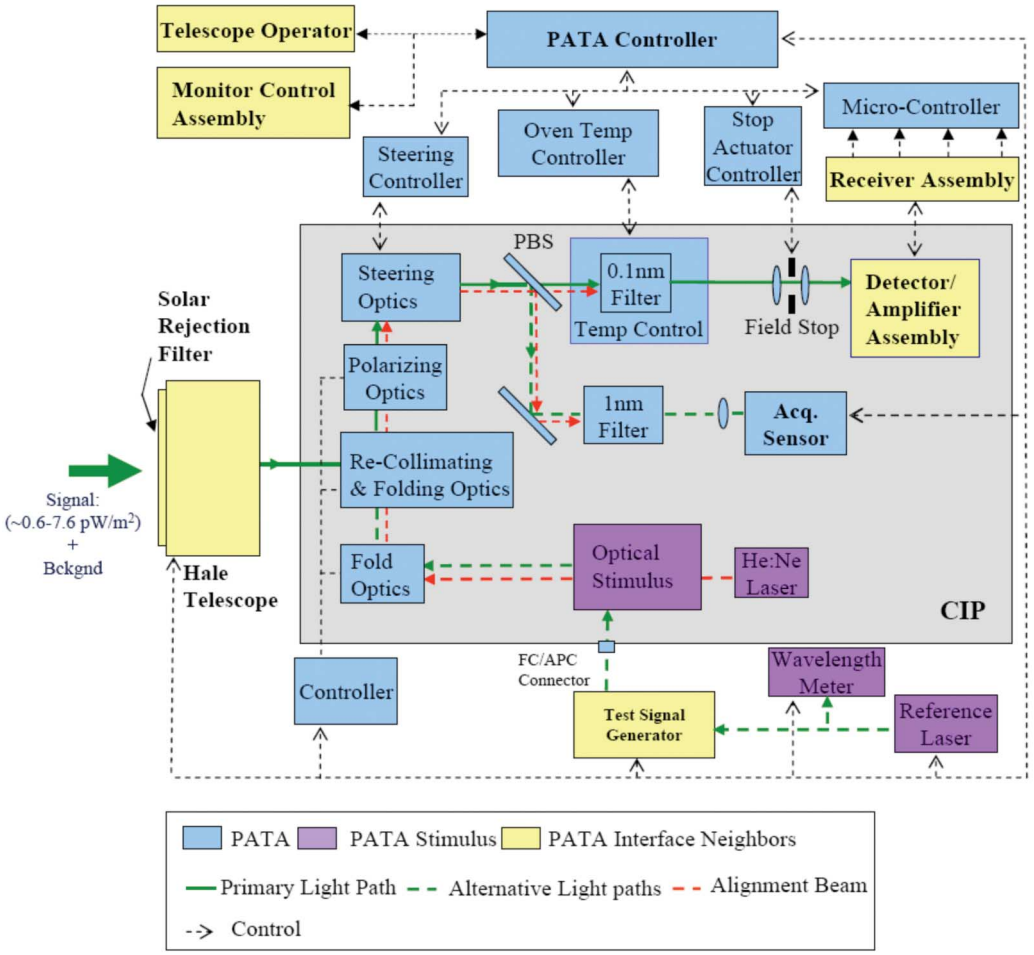

Fig. 5. ***PATA block diagram showing the different light paths described in the text above. The dashed black lines indicate the intrasystem interfaces within PRT that are controlled and monitored.***

occur (see Section III-D). Prior to temporal acquisition, incidence of downlink on the detector would be open loop, necessitating the wide open field-stop. Following temporal acquisition (< 60 s), the RA would feed back mean-signal estimates to a microcontroller, where a spatial error signal used to close a line-of-sight stabilization loop would be extracted. In other words, signals fed to the steering optics would keep the signal spot centered in the field-stop. At this stage, the field-stop would also be adjusted to optimize the operating point (see Section II). Fig. 6 shows a summary of the PATA sequence of events.

C. Detector Amplifier Assembly (DAA)

The DAA would conduct photoelectric conversion and signal conditioning for subsequent processing by the RA. The DAA would incorporate a test signal generator (TSG) to emulate the MLT laser signal for testing. Driving requirements for the detector were:

i) to provide a photon-detection efficiency (PDE) greater than 30% at 1064 nm;
ii) to display a gain variance less than 10%;
iii) to output single photon pulse-widths of 1 ns measured at 10% nominal pulse height;
iv) to provide a quadrant configuration with four analog outputs;

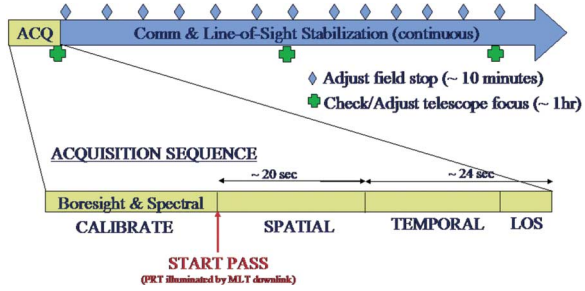

Fig. 6. ***Operational sequence summary for PATA.***

v) to provide an FOV of 10–15 μrad measured on the sky, corresponding to half of the quadrant detector diameter;
vi) to have a lifetime of at least 1000 h.

After a thorough evaluation of available options for achieving high photodetection efficiency at 1064 nm, a hybrid photodiode (HPD) utilizing an InGaAsP photocathode was selected. The InGaAsP photocathode HPD was manufactured by Intevac Inc., Santa Clara, CA. The anode is a GaAs Schottky avalanche diode.

The detector was not a commercially available item, and development was pursued through a program that involved testing of mostly custom devices. The incident signal plus background photon flux, especially during near-Sun operations, would be high, driving a single detector to saturation. Splitting the incident photon-flux over a quadrant configuration solved this problem while facilitating the extraction of an error signal for the line-of-sight stabilization and control mentioned in Section III-B.

Output pulse widths of 450 ps were measured in the laboratory while PDE of greater than 30% was achieved with the HPD at temperatures less than 250 K. Dark currents were measured at 250 Kcps at a temperature of 224 K. Count rates of 200 Mcps were achieved with a Jet Propulsion Laboratory custom threshold circuit. The operating bandwidth for this circuit was 3 GHz. The outputs from the four quadrants of the HPD were fed into low-noise preamplifiers maintained at the detector temperature inside a detector cryostat module. Feeds from the preamplifiers were fed to room temperature low-noise postamplifiers. A schematic block diagram of the DAA is shown in Fig. 7.

The auxiliary electronics, diagnostics, and control needed by the DAA are shown in Fig. 7, including the TSG. In this paper, the TSG is not discussed. The analog signal output (four channels) shown in Fig. 7 was to be fed to the receiver assembly, described next.

D. Receiver Assembly (RA)

The driving requirements for the receiver were:

i) to perform data frame, slot, symbol, and code-word synchronization functions, not necessarily in the stated order;
ii) to accomplish temporal acquisition in less than 60 s for an initial 1-part-per-million frequency offset;
iii) to provide the capability to maintain temporal tracking at outages up to 30 ms;
iv) to incur implementation losses, measured at the output of the decoder and relative to an ideal Poisson photon counting receiver of less than 0.8 dB;
v) to deinterleave the data frame into individual code words.

The receiver converted the analog output from the detector into counts via digital thresholding with a custom photon discriminator, deserializer interface. This unit essentially used a 1-bit analog-to-digital converter running at 3 Gs/s, with a 1-dB compression of photon-count rates for 250 Mcps. Through simulations and laboratory tests receiver losses of less than 0.8 dB at representative operating points (n_s and n_b combinations) spanning the mission profile were verified. Slot synchronization, one of the most challenging functions, was accomplished on each individual channel of received data prior to combining with the aid of a "training" sequence of pulses inserted into the transmitted data streams. This was found to be a low-risk implementation with a modest impact on overall data throughput of less than 4%. Parameter estimation—used to determine the channel operating point—would be used for three different functions in the receiver: i) computation

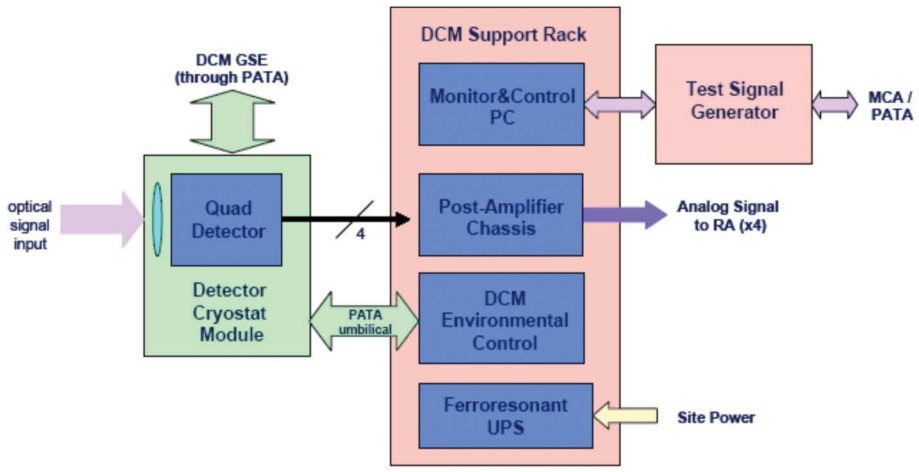

Fig. 7. *Schematic block diagram of the detector amplifier assembly.*

of the likelihood ratio for input to the decoder assembly, ii) PATA feedback for closing line-of-sight stabilization loop, and iii) receiver status monitor functions.

For the sake of brevity, a high-level functional description depicted in Fig. 8 is presented. The modulated laser signal $u(t)$ is composed of PPM modulated laser signal flux n_s and background flux n_b. The horizontal direction represents time with blue vertical markers representing PPM-word boundaries and black vertical markers denoting PPM-slot boundaries. An $M = 4$ slot PPM-word with the laser-pulse slot denoted by a square pulse is shown in the first line of Fig. 8. Photon arrivals are shown in the second line of Fig. 8, where additive noise photons can arrive in any of the nonsignal or signal slots. In the third line, photon arrivals are converted to an analog electrical signal $s(t)$ following photoelectric conversion and amplification at the DAA (see Section III-C). These bandlimited pulses represent signal and background flux and other additive noise such as detector dark response. The pulses are bandlimited to approximately 2 GHz. The receiver samples $s(t)$ are then converted to estimated photon counts per slot period $\hat{k}_m$, illustrated in the fourth line in Fig. 8. The unsynchronized photon counts are synchronized to slot boundaries as illustrated conceptually on line 5 (other forms of synchronization are also performed but omitted here for the sake of simplicity). The signal and background flux $(n_s + n_b)$ per slot are estimated as indicated in lines 6 and 7. Parameter estimates are used to create log-likelihood ratios that are output to the decoder. The signal and background estimates are also passed to the PATA and MCA.

E. Decoder Assembly

The decoder assembly would accept slot and codeword-synchronized photon counts from the RA to produce estimates of the user bit stream as well as error flags for codewords that the decoder could not recover. The performance of the decoder assembly is measured by the codeword error rate (WER), bit error rate (BER), and undetected error rate (UER), i.e., the fraction of codewords erroneously declared correct. The driving requirements for the decoder assembly were:

i) to provide performance within 1.2 dB of the ideal Poisson channel capacity at a WER of 10^{-4};
ii) to provide an error flag with a UER of less than 10^{-9} wherever the WER is less than 10^{-4};
iii) to interface with both $M = 32$ and $M = 64$ PPM;
iv) to produce a decoded bit stream at rates up to 50 Mbps.

Several classes of codes were considered for the error-correction code: hard-decision-decoded Reed–Solomon codes [18], [19], parallel concatenated convolutional [20]–[23], serially concatenated convolutional [24]–[26], and low-density parity-check (LDPC) [27], [28].

The serial concatenated PPM (SCPPM) code described in [24] was found to provide the best performance. This code treats PPM as the inner code in a serial concatenation with a short constraint length convolutional code.

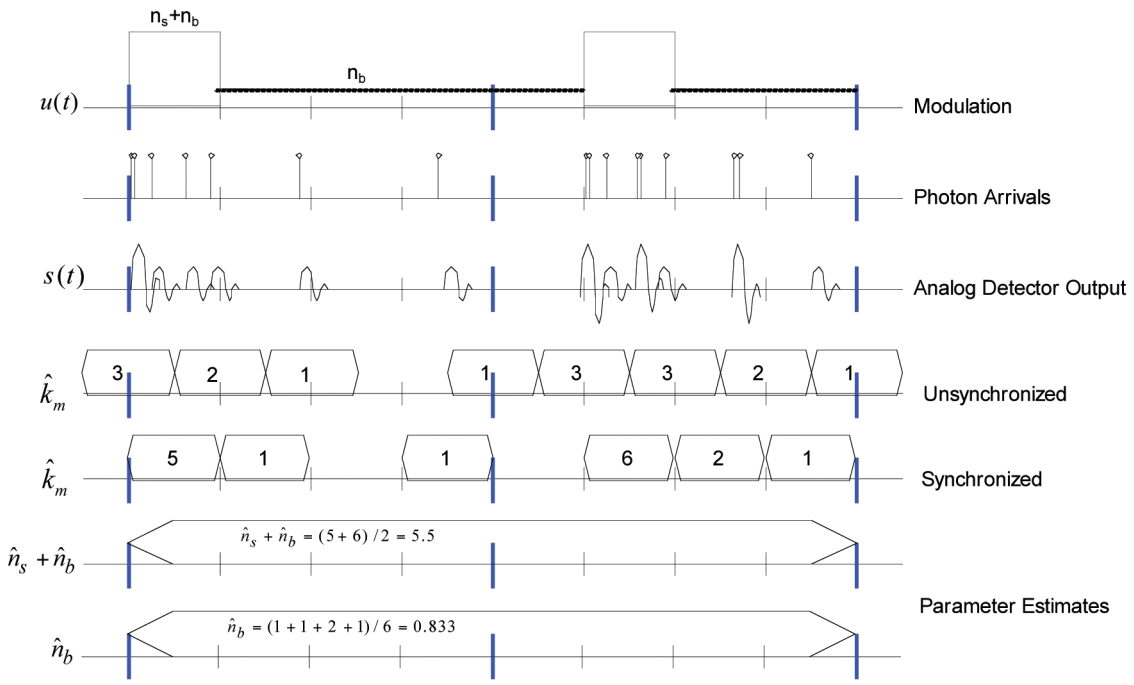

Fig. 8. *Signal flow diagram for the receiver assembly. The horizontal direction represents time, with the black graduation marks denoting slots of 1.6 ns and the blue graduation marks denoting PPM-word boundaries of 64 times the slot width.*

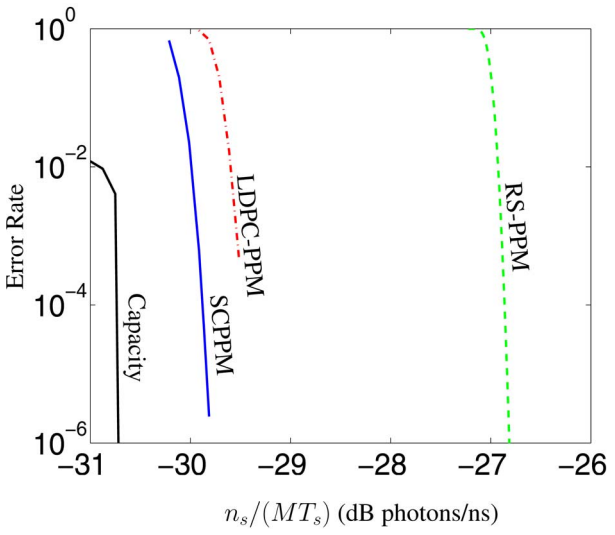

Fig. 9. *SCPPM, LDPC-PPM, and RS-PPM performance $M = 64$, $n_b = 0.2$, $T_s = 32$ ns.*

Using extrinsic information transfer function analysis [29], we chose a memory 2 [octal taps (5, 7)], rate 1/2 convolutional code. A recursive $1/(1 + D)$ binary accumulator is added prior to the PPM mapping in the signaling chain improve the performance of iterative decoding. In the decoder the PPM mapping and binary accumulator are decoded jointly.

A longer bit-interleaver provides better performance (although with diminishing gains) but requires larger memory to implement. An interleaver length of $15\,120 = 2^4 \times 3^3 \times 5 \times 7$ bits was chosen as a good tradeoff between performance and complexity. This value is divisible by $\log_2 M$ for a large range of M, allowing easy integration with various PPM orders. The interleaver was based on a quadratic permutation polynomial [30], and we observed no loss in performance relative to a pseudorandom spread interleaver. Simulation and bounds [31] on the performance illustrated error floors would be far below 1E-8, with negligible impact for our purposes.

Fig. 9 illustrates floating-point performance at a nominal operating point of the SCPPM code and two leading alternatives: an iteratively demodulated (LDPC) code and RS-coded PPM. In all cases, the code is designed to "fit" the modulation, and the LDPC codes and SCPPM both iteratively demodulate, essentially treating the modulation as part of the ECC. This matching is critical to obtain near-capacity performance. The SCPPM code gained 4.8 dB over the noniterative RS code and was within less than 1-dB of capacity over a wide range of operating points for the deep-space Mars link—with moderate encoding and decoding complexity.

Although LDPC codes have proven to have performance comparable to or better than turbo-like codes on the Gaussian channel, none of our LDPC code designs outperformed SCPPM. Furthermore, for deep-space channels, the onus on complexity lies with the space-based encoder more so than with the Earth-based decoder, and LDPC encoders have higher complexity than the SCPPM encoder. At the time of selection, performance, technology maturity, and complexity factors favored the SCPPM code.

F. Monitor and Control Assembly (MCA)

The MCA would be distributed over the entire MLCD ground network providing monitoring, control, and coordination. Commands to the MLT through the MTO mission operations system would also be coordinated by the MCA. The monitor and control process at the PRT centered about a MySQL database that would contain orbital predicts, command sequences, and all the data produced by other PRT assemblies. The MLCD MOS accesses the database as a client to transmit commands and predicts and receives operational status. Local display terminals at PRT also acted as clients to the database server. Fig. 10 is a block diagram representation the configuration described. The PRT MCA contained a data-processing assembly to receive and store decoder assembly

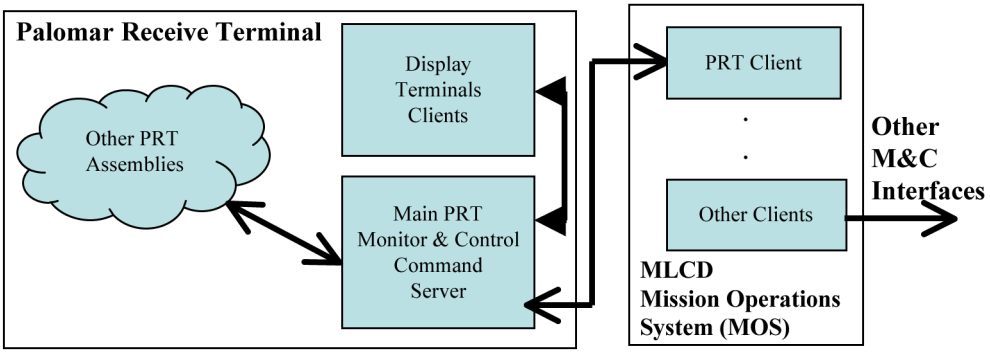

Fig. 10. *Depicting the server client configuration used for monitor and control of PRT.*

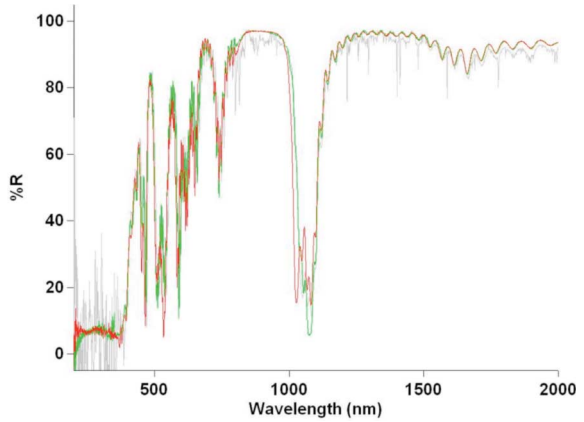

Fig. 11. *Reflection spectra from the membrane filter at various radial positions.*

output and create virtual channels for MLT telemetry and science data. A separate MySQL database would have stored the downlink data from MLT.

IV. TECHNOLOGY VALIDATION

A. Telescope Assembly Validation

Validation of the telescope assembly was considerably simplified and shortened by making use of an existing, well-characterized telescope and the Palomar High Angular Resolution Observer (PHARO) [32] instrument. What remained were tests to validate the membrane filter technology and tests to validate operation of the telescope under the very specific, unusual conditions expected to arise during MLCD operations. These latter tests were limited to operations during and after extreme sun exposure to assure that the telescope could continue to perform within operational requirements.

Among the technology elements with lowest "readiness" was the membrane filter, which had to be taken from the concept level to operational readiness. During the period of MLCD performance, the CP1 substrate material was manufactured and tested, optically as well as mechanically, to assure that it could withstand the stresses of the exposed telescope environment. In parallel, the filter coatings were developed and applied over large surface areas. A 1.5-m prototype was created for initial feasibility testing. Difficulties with deposition rate control among the various thin-film layers led to slight point-to-point variations in spectral performance, as Fig. 11 shows. This in turn resulted in radial variations in transmission shown in Fig. 12.

The average filter transmission measured after placement over a 1-m telescope aperture at the Optical Communications Telescope Laboratory, Wrightwood, CA, was 48% in the 1.059–1.069-μm spectral band, lower than the targeted 78%. We anticipate that with further process control development, average in-band optical throughput can be improved to exceed 80%. Using the same test arrangement and multiple time-exposure images of the star Betelgeuse further demonstrated that there was no noticeable filter-induced degradation to the full width at half-maximum (FWHM) blur size beyond the 10.9 μrad seeing-limited observations, validating predictions of excellent optical performance.

Stray light from the Hale telescope primary mirror was validated by performing experiments that involved pointing close to the Moon instead of the Sun and used the PHARO instrumentation [33]. Validation of the 200-in Hale telescope operation under stressing thermal conditions was performed by opening the telescope dome and exposing the telescope and dome interior to sunlight for a full 8-h day around the summer solstice. Thermal sensors were used to acquire infrared imagery for monitoring heating of telescope and dome structures. A maximum temperature rise of almost 60 °C was recorded in some cases. Monitoring of the concrete dome floor, the telescope right-ascension bearing, prime focus secondary spider, and primary mirror cell all showed thermal rises exceeding any

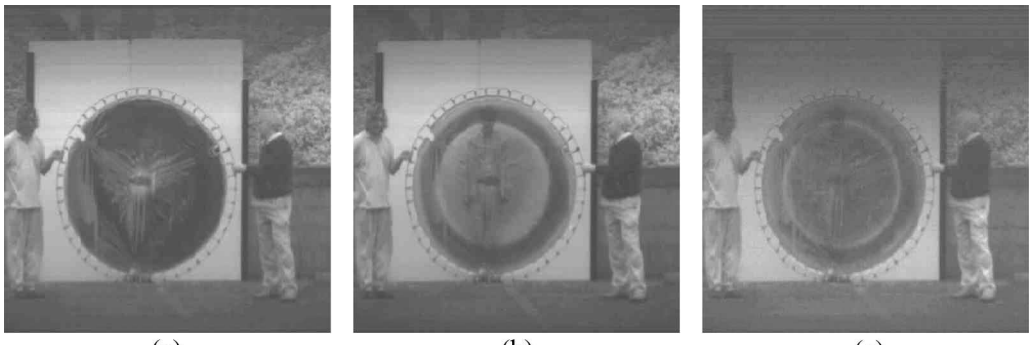

Fig. 12. *Narrow-band images of one of the authors through the 1.5-m7p membrane filter at (a) 990, (b) 1064, and (c) 1102 nm. Errors during the deposition run resulted in changes to the spectral transmission band of the outer ring of the filter.*

ever previously noted within a 24-h period. At the conclusion of this exposure (though still during daylight hours), the telescope was pointed toward objects in the eastern sky and images recorded using the PHARO instrument mounted in the Cassegrain cage. In spite of these excessive thermal changes, the telescope generated seeing-limited images of 7.8 μrad (FWHM on a 14-s exposure) at 4:00 PM local time (LT), dropping to 3.4 μrad immediately after sunset and ultimately 0.97 μrad with the adaptive optics system operating later during the same night. The blind-pointing accuracy of the telescope likewise suffered little if any degradation as a result of the thermal exposure. During the afternoon after telescope exposure, the blind pointing accuracy was measured to be 26.7 μrad, dropping to 24.2-μrad soon after sunset, identical in magnitude to the measurements taken the night prior to Sun exposure. While firm conclusions regarding the ability of the telescope to withstand and operate after repeated daytime exposure should only be drawn after much more testing, it is at least clear that the greatest concerns of telescope seeing and pointing ability are not catastrophic to operations or to subsequent astronomical use of the telescope.

B. Detector/Receiver/Decoder Validation

To validate the design of the PRT backend (detector, receiver, decoder), a laboratory test setup was assembled. This is shown in Fig. 13. Using a video camera as the data input, an end-to-end detection, demodulation, and decoding scheme was constructed as described below.

The camera footage is first compressed by a hardware MPEG-2 encoder. This MPEG stream is then sent via TCP/IP to a desktop personal computer running a software SCPPM encoder.

A 64-ary PPM mapper takes in the encoded SCPPM symbol stream and modulates a ytterbium (Yb)-doped 10-KHz spectral width fiber laser operating at 1064 nm. The modulated PPM pulses are then sent over a length of fiber to the HPD detector. The HPD detector generates bandlimited pulses for each photon detected. The receiver assembly performs slot synchronization and computes an estimate of the photon count in a PPM slot, according to the magnitude of the bandlimited signal. The receiver assembly proceeds to use photon count estimates to calculate PPM symbol log-likelihood ratios, which are fed to the decoder assembly. Both the receiver and decoder were implemented using Xilinx Virtex II field-programmable gated arrays (FPGAs). The SCPPM decoded bit stream was then MPEG decoded to recover the original camera video output prior to displaying the video stream.

The performance of the end-to-end system is plotted in Fig. 14. Two experimental runs operating at 4 and 6 Mbps are shown. Both use only the top eight (out of 64) channel statistics [34] and a maximum of seven SCPPM decoding iterations. The two curves compare closely to a standalone FPGA-based decoder assembly simulated with seven iterations. A simulated FPGA based decoder with full 64-slot statistics and a maximum of 32 iterations is also shown. The curves show that the partial statistics and a maximum of seven iterations led to a 0.6 dB loss of

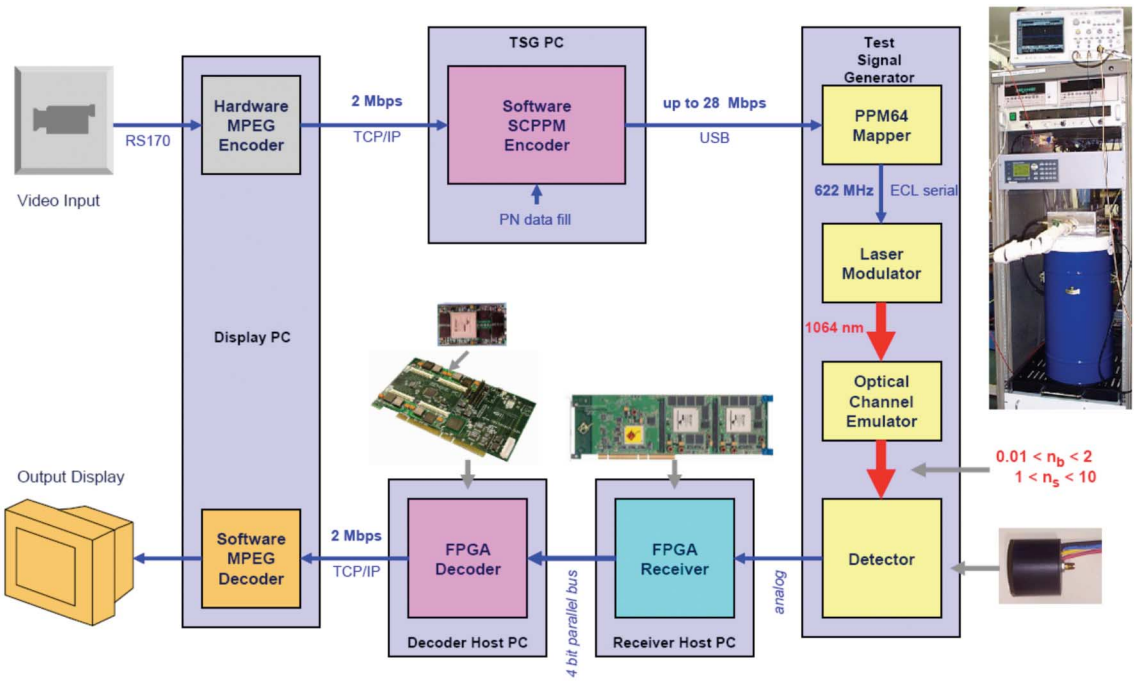

Fig. 13. *Test setup for an end-to-end validation of detection and demodulation.*

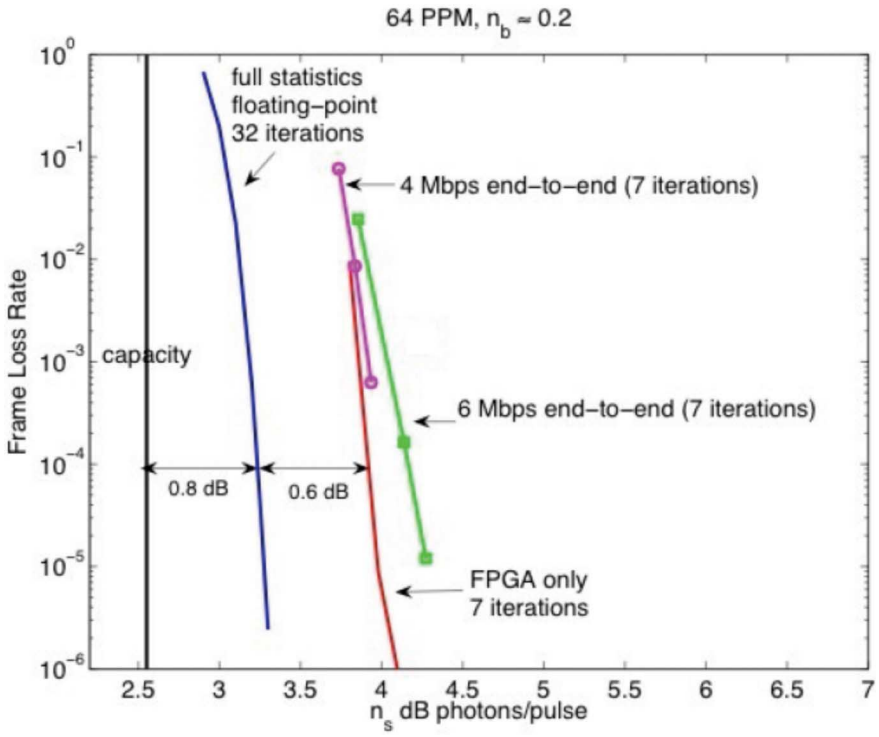

Fig. 14. ***End-to-end system performance. A frame is 7560 information bits and 15 120 codeword bits.***

performance. The end-to-end performance is also shown to be within 1.4 dB of Shannon capacity. At a frame loss rate of 10^{-5}, the number of signal photons per pulse slot is 2.67, corresponding to 1.12 information bits per photon.

V. CONCLUSION

A description of the preliminary design of the PRT along with critical technology validation test results was presented. MLCD was to have been the first attempt at communicating optically over planetary distances. The advances described in the PRT design would have enabled satisfying the data rates that the Mars link demonstration was targeting. The interest in deep-space optical communications persists [35]–[37]; however, technology validation demonstrations are needed to retire risks associated with implementing a new technology. Therefore, "PRT-like" designs, where an existing infrastructure is suitably retrofitted for technology demonstrations, may prove to be cost-effective stepping stones towards an eventual operational implementation of deep-space optical communications. ■

Acknowledgment

The authors are indebted to C.-C. Chen for excellent technical guidance throughout the PRT design effort. They gratefully acknowledge programmatic guidance from M. Aung, B. Parvin, and S. Townes of the Jet Propulsion Laboratory. Technical assistance from R. Barron, D. Boroson, L. Candall, and F. Khatri of MIT Lincoln Laboratory is gratefully acknowledged. Thanks are due to B. Edwards, R. Fitzgerald, and R. Jenkens of NASA Goddard Space Flight Center for valuable insights and guidance. The authors would like to thank R. DePaula of NASA headquarters for his support and guidance. They are thankful for the assistance from Caltech Optical Observatories: A. Pickles, K. Matthews, H. Petrie, and R. Thicksten. Finally, they would like to thank R. Dekany and M. Troy for making the PHARO instrument available on numerous occasions.

REFERENCES

[1] B. L. Edwards *et al.*, "Overview of the Mars laser communications demonstration project," presented at the AIAA Space Conf. 2003, 2003, paper 2003-6417.

[2] D. Boroson, A. Biswas, and B. L. Edwards, "MLCD: Overview of NASA's Mars laser communications demonstration system," in *Proc. SPIE Free-Space Laser Commun. Technol. XVI*, G. S. Mecherle, C. Y. Young, and J. S. Stryjewski, Eds., 2004, vol. 5338, pp. 16–28.

[3] S. Townes *et al.*, "The Mars laser communication demonstration," in *Proc. IEEE Aerosp. Conf.*, Mar. 6–13, 2004, vol. 2, pp. 1180–1195.

[4] A. Biswas, D. Boroson, and B. L. Edwards, "Mars laser communication demonstration: What it would have been," in *Proc. SPIE Free-Space Laser Commun. Technol. XVI*, G. S. Mecherle, Ed., 2006, vol. 6105, pp. 610502-1–6105052-12.

[5] J. J. Scozzofava, D. M. Boroson, R. S. Bondurant, A. D. Pillsbury, J. W. Burnside, N. W. Spellmeyer, P. L. Ward, F. K. Knight, M. L. Stevens, and D. R. Bold, "The Mars Lasercom terminal," *2005 Dig. LEOS Summer Topical Meeting*, 2005, paper MA1.2.

[6] J. W. Burnside, D. V. Murphy, F. K. Knight, and F. I. Khatri, "A hybrid stabilization approach for deep-space optical communication," *Proc. IEEE*, vol. 95, no. 10, pp. 2070–2081, Oct. 2007.

[7] S. F. Franklin *et al.*, "The 2009 Mars Telecom Orbiter mission," in *Proc. IEEE Aerosp. Conf.*, Mar. 6–13, 2004, vol. 1, pp. 437–456.

[8] C.-C. Chien, A. Biswas, W. T. Roberts, and M. J. Britcliffe, "Turning Palomar into a deep-space optical receiver," presented at the 2005 Digest of the LEOS Summer Topical Meetings, Paper MA 1.3.

[9] L. M. Candall, "LDES: A prototype array optical receiver for the Mars laser communication demonstration program," presented at the 2005 Digest of the LEOS Summer Topical Meetings, Paper MA 2.

[10] J. A. Mendenhall, L. M. Candell, P. I. Hopman, G. Zogbi, D. M. Boroson, D. O. Caplan, C. J. Digenis, D. R. Hearn, and R. C. Shoup, "Design of an optical photon counting array receiver system for deep space communications," *Proc. IEEE*, vol. 95, no. 10, pp. 2059–2069, Oct. 2007.

[11] A. Biswas and S. Piazzolla, "Deep-space optical communications downlink budget from Mars: System parameters," IPN Prog. Rep. 42-154, Aug. 15, 2003.

[12] B. Moision and J. Hamkins, "Deep-space optical communications downlink budget: Modulation and coding," IPN Prog. Rep. 42-154, Aug. 15, 2003.

[13] H. Hemmati, A. Biswas, and D. Boroson, "Prospects for improvement of interplanetary laser-communication data rates by 30-dB," *Proc. IEEE*, vol. 95, no. 10, pp. 2082–2092, Oct. 2007.

[14] W. T. Roberts, H. L. Petrie, A. J. Pickles, R. P. Thicksten, and C. Echols, "Feasibility of utilizing the 200-inch Hale telescope as a deep-space optical receiver," in *Proc. SPIE Free-Space Laser Commun. IV*, J. C. Ricklin and D. G. Voelz, Eds., 2004, vol. 320–335, p. 5550.

[15] B. G. Patrick, P. Gierow, D. Sheikh, and W. T. Roberts, "Solar filter for Mars laser communication demonstration optical receiver," in *Proc. SPIE Free-Space Laser Commun. IV*, J. C. Ricklin and D. G. Voelz, Eds., 2004, vol. 336–343, p. 5550.

[16] W. T. Roberts, "Optical membrane technology for deep-space optical communications filters," presented at the Proc. IEEE Aerosp. Conf., 2005, paper 1209.

[17] A. Biswas, S. Piazzolla, K. Quirk, G. G. Ortiz, S. Lee, M. Sriniviasan, and C. C. Chen, "Approach for acquiring and tracking downlink from Mars using the Hale telescope," in *Proc. SPIE Free-Space Laser Commun. Technol. XVII*, G. S. Mecherle, Ed., 2005, vol. 60–71, p. 5712.

[18] R. J. McEliece, "Practical codes for photon communication," *IEEE Trans. Inf. Theory*, vol. IT-27, pp. 393–398, Jul. 1981.

[19] J. Hamkins and B. Moision, "Performance of long blocklength Reed-Solomon codes with low order pulse position modulation," *IEEE Trans. Commun.*, submitted for publication.

[20] C. Berrou and A. Glavieux, "Near optimum error correcting coding and decoding: Turbo-codes," *IEEE Trans. Commun.*, vol. 44, pp. 1276–1271, Oct. 1996.

[21] K. Kiasaleh, "Turbo-coded optical PPM communications systems," *J. Lightw. Technol.*, vol. 6, pp. 18–26, Jan. 1998.

[22] J. Hamkins, "Performance of binary turbo-coded 256-PPM," TMO Prog. Rep., Aug. 1999, vol. 42, pp. 1–15.

[23] M. Peleg and S. Shamai, "Efficient communication over the discrete-time memoryless Rayleigh fading channel with turbo coding/decoding," *Eur. Trans. Telecommun.*, vol. 11, pp. 475–485, Sep.–Oct. 2000.

[24] B. Moision, J. Hamkins, and M. Cheng, "Design of a coded modulation for deep-space optical communications," in *Proc. Inf. Theory Applicat. Workshop*, La Jolla, CA, Jan. 2006.

[25] J. L. Massey, "Capacity, cutoff rate, and coding for a direct-detection optical channel," *IEEE Trans. Commun.*, vol. COM-29, pp. 1615–1621, Nov. 1981.

[26] S. Benedetto, D. Divsalar, G. Montorsi, and F. Pollara, "Serial concatenation and inteleaved codes: Performance analysis, design and iterative decoding," *Telecommun. Data Acquisition Prog. Rep.*, vol. 42-126, Aug. 1996.

[27] M. Barsoum and B. Moision, "An LDPC code for optical space communication," Jet Propulsion Laboratory, Tech. Rep., Oct. 2005.

[28] S. Brink, G. Kramer, and A. Ashikhmin, "Design of low-density parity-check codes for modulation and detection," *IEEE Trans. Commun.*, vol. 52, pp. 670–678, Apr. 2004.

[29] S. Brink, "Convergence of iterative decoding," *Electron. Lett.*, vol. 35, pp. 806–808, May 1999.

[30] J. Sun and O. Y. Takeshita, "Interleavers for turbo codes using permutation polynomials over integer rings," *IEEE Trans. Info. Theory*, vol. 51, pp. 101–119, Jan. 2005.

[31] B. Moision and J. Hamkins, "Error rate bounds for coded PPM on the Poisson channel," *IEEE Trans. Commun.*, submitted for publication.

[32] R. Dekany, K. Wallace, G. Brack, B. R. Oppenheimer, and D. Palmer, "Initial test results from the Palomar 200," in *Proc. SPIE Adaptive Opt. Syst., Adaptive Opt. Applicat.*, R. K. Tyson and R. Q. Fugate, Eds., 1997, vol. 3126, pp. 269–276.

[33] W. T. Roberts, "Stray-light observations at the Hale telescope on Palomar mountain," in *Proc. IEEE Aerosp. Conf.*, Mar. 5–12, 2005, pp. 1612–1620.

[34] B. Moision and J. Hamkins, "Reduced complexity decoding of coded PPM using partial statistics," in *JPL IPN Prog. Rep.*, vol. 42-161, 2005.

[35] J. S. Schier, J. J. Rush, W. D. Williams, and P. Vrotsos, "Space communication architecture supporting exploration and science: Plans and studies for 2010–2030," in *1st Space Exploration Conf. Continuing Voyage Discovery*, Orlando, FL, Jan. 30–Feb. 1, pp. 1–33, AIAA 2005-2517.

[36] R. J. Cesarone, D. S. Abraham, and L. J. Deutsch, "Prospects for a next generation deep space network," *Proc. IEEE*, vol. 95, Oct. 2005.

[37] W. D. Williams *et al.*, "RF and optical communications: A comparison of high data rate returns from deep space in the 2020 timeframe," in *Proc. 12th Ka Broadband Commun. Conf.*, Naples, Italy, Sep. 2006, paper K000083.

ABOUT THE AUTHORS

Abhijit Biswas received the Ph.D. degree from Southern Illinois University at Carbondale.

He is a Senior Telecommunication Engineer with California Institute of Technology, Jet Propulsion Laboratory (JPL), Pasadena. He has worked in the areas of laser spectroscopy and free-space laser communications for the past 20 years. He is currently with the Optical Communications Group, JPL. He was the Ground Network Systems Engineer for the Mars Laser Communication Demonstration Project.

Bruce Moision received the B.S. degree in engineering from Harvey Mudd College, Claremont, CA, in 1991 and the Ph.D. degree in electrical and computer engineering from the University of California, San Diego, in 1999.

From 1991 to 1994, he was with Datatape, Inc., Pasadena, CA. During 2000, he held a postdoctoral position with the Mathematics of Communications Research Group, Lucent Technologies, Murray Hill, NJ. He has been with the Information Processing Group, Jet Propulsion Laboratory, Pasadena, since 2001.

William T. Roberts received the B.S. and M.S. degrees in physics from the University of Alabama in Huntsville and the M.S. and Ph.D. degrees in optical sciences from the University of Arizona, Tucson.

He is a Senior Member of the Technical Staff, Optical Communications Group, Jet Propulsion Laboratory, Pasadena, CA, where he was the Cognizant Engineer for the Telescope Assembly on the Mars Laser Communication Demonstration Project. He has worked on development of optical systems and laser transmitters for deep-space optical communication systems as well as infrared system design and sodium guide star laser development for adaptive optics. He previously was with Nichols Research Corporation in development of LWIR infrared detectors and infrared systems, in positions from Research Scientist to Associate Fellow Member of the Technical Staff.

William H. Farr is presently Manager of the Optical Communications Technology Program, Jet Propulsion Laboratory (JPL), Pasadena, CA, and is concurrently pursuing research and development on photon counting detectors for high-data-rate deep space optical communications. Prior to joining JPL in 2001, he operated his own business developing high-power diode laser electronics and nonlinear optical systems including optical parametric oscillators and amplifiers and sum-frequency mixing for infrared signal detection and imaging. Shortly after arriving at JPL, he established the Deep Space Optoelectronic Detector Characterization Facility to promote development of photon counting detector technologies to meet optical communications requirements. He was the Cognizant Engineer for the ground-based detector system for the Palomar Receive Terminal, Mars Laser Communications Demonstration project.

Andrew Gray, photograph and biography not available at the time of publication.

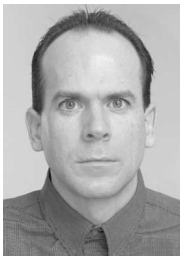

Kevin Quirk received the B.S. degree in computer engineering and the M.S. and Ph.D. degrees in electrical engineering from the University of California at San Diego, La Jolla, in 1993, 1997, and 2000, respectively.

From 2000 to 2002, he was with the Jet Propulsion Laboratory (JPL), Pasadena, CA, as a Member of the Digital Signal Processing Research Group. From 2003 to 2004, he was a Postdoctoral Researcher with the Department of Electrical Engineering, University of California, San Diego. Since 2004, he has been a Contractor with the Communication Systems and Research Section, JPL. He was a Lecturer at the University of California, Los Angeles and the University of California at San Diego, and is currently a Lecturer with the Department of Electrical Engineering, California Institute of Technology, Pasadena. His research interests include communication theory, coding theory, signal processing, free space optical communications, and spread-spectrum communications.

Jon Hamkins received the B.S. degree in electrical engineering from California Institute of Technology, Pasadena, in 1990 and the M.S. and Ph.D. degrees in electrical and computer engineering from the University of Illinois at Urbana-Champaign in 1993 and 1996.

Since then, he has been with the Jet Propulsion Laboratory, Pasadena, where he is now the Supervisor of the Information Processing Group.

Michael K. Cheng received the B.S. degree from Carnegie-Mellon University, Pittsburgh, PA, in 1995, the M.S. degree from The University of Texas at Austin in 1997, and the Ph.D. degree from the University of California, San Diego, in 2004, all in electrical and computer engineering. Since then, he has been with the Information Processing Group, JPL, working on design and efficient implementation of modern error-correcting codes.

Jonathan Gin received the B.S. degree in electrical engineering with an emphasis in computer science from the University of California, Los Angeles, in 2002 and the M.S. degree in electrical engineering from Stanford University, Stanford, CA, in 2004.

He is a Member of Technical Staff with the Signal Processing Research Group, Jet Propulsion Laboratory, Pasadena, CA. His interests reside in communications signal-processing algorithms along with FPGA design and implementation. He currently is working on receiver development for wide-band RF and optical communication systems.

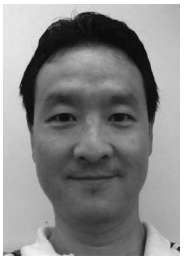

Michael Nakashima received the B.S. degree in electrical engineering from the University of Hawaii at Manoa.

He has 17 years of experience designing digital flight hardware and ground support equipment. He has been with the Jet Propulsion Laboratory for the past eight years and has supported various flight projects including Mars Exploration Rover and DAWN. He is currently designing support equipment for the Mars Science Lander due to launch in 2009.

Gerardo G. Ortiz received the B.S. degree in electrical engineering from the University of California, Los Angeles, in 1986 and the M.S.E.E. and Ph.D. degrees in optoelectronics from University of New Mexico, Albuquerque, in 1993 and 1997, respectively.

After receiving the bachelor's degree he was with the Jet Propulsion Laboratory (JPL), Pasadena, CA, for five years developing ultra-low-noise high electron mobility transistor microwave amplifiers for NASA's Deep Space Network. His graduate work included studies in device physics, semiconductor lasers, resonant cavity detectors, and optical communication. Upon graduation he returned to JPL, where he is currently a Senior Member of the Engineering Staff involved in all aspects of the development of free-space optical communications. His current research emphasis includes high-precision laser beam pointing, algorithm and system development for the acquisition and tracking of dim sources from deep space distances, and component development in photon counting arrays, low-noise high update rate inertial reference units, and star trackers.

Sabino Piazzolla received the laurea degree in electrical engineering from the University of Rome "La Sapienza" and the M.S.E.E. and Ph.D. degrees from the University of Southern California (USC), Los Angeles.

He was a Researcher with the Integrated Multimedia Systems Center, USC. He was with the Microwave System Group, Alenia Spazio, where he participated in a number of international space program such as ERS1, ITALSAT, and SARX. Currently he is with the Optical Communication Research Group, Jet Propulsion Laboratory, Pasadena, CA. His fields of interest are microwave, optical communication, optical computing, optical storage, and atmospheric optics. He is also currently a Lecturer at USC.

Carl Christian Liebe received the M.S.E.E. and Ph.D. degrees from the Department of Electrophysics, Technical University of Denmark, in 1991 and 1994, respectively.

Since 1997, he has been with the Jet Propulsion Laboratory, California Institute of Technology, Pasadena, CA. Currently, he is a Senior Member of the Active Optical Sensing Group. He was the Cognizant Engineer for PATA. He has authored/coauthored more than 50 papers.

Dr. Liebe has received more than 30 awards.

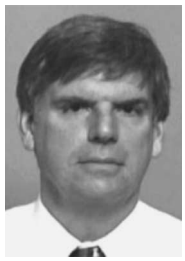

David L. Losh received the B.S. degree in physics from Case Institute of Technology, Cleveland, OH, in 1970 and the M.S. degree in computer science from University of Southern California, Los Angeles, in 1980.

As a Senior Telecommunications Engineer with the Communications Ground Systems Section, Jet Propulsion Laboratory, Pasadena, CA, he was the Cognizant Development Engineer for the monitor and control subsystem described in this paper.